COBEM 2023 27TH INTERNATIONAL CONGRESS OF MECHANICAL ENGENEERING

ABCM Brazilian Society of Mechanical Sciences and Engineering
27th ABCM International Congress of Mechanical Engineering
December 04-08, 2023, Florianópolis-SC, Brazil

COBEM2023-2231
EVALUATION OF "MICRO-CLADDING" PARAMETERS IN FACE OF THERMAL EFFECTS REDUCTION FOR TOP-HAT LASERS

Joares L. dos Reis
Paulo P. O. L. Dyer
Faculdade de Tecnologia do Estado de São Paulo. Instituto de Estudos Avançados EFO/IEAv
joares.lidovino@fatec.sp.gov.br; paulo_dyer@yahoo.com
Silvelene A. Silva
Instituto Nacional de Pesquisas Espaciais INPE/LAS
lenisoni@uol.com.br

Helder de P. Vicente
Instituto de Estudos Avançados EFO/IEAv
helder.10@hotmail.com
Andersan dos Santos Paula
Danilo Abílio Corrêa Gonçalves
Naiara Vieira Le Sénéchal
Instituto Militar de Engenharia
andersan@ime.eb.br
Getúlio de Vasconcelos
Instituto de Estudos Avançados EFO/IEAv
getuliovas@gmail.com

Abstract. *Coating or additive manufacture by laser cladding supply a wide range of industrial and technological applications. However, laser energy may compromise the substrate microstructure, according to beam profiling. Whereas in the Gaussian the energy decreases symmetrically; top-hat provide, in theory, a constant energy from the target. Nevertheless, as observed, in practice top-hat lasers provide a central small energy peak. Producing an extra melt area (A_p), under the substrate melting area (A_m). In this context, this paper aimed the parameters obtention of efficiency (E); associated to laser power (P); velocity of scanning (v_s) and powder feeding rate (μ) in order to establish a concept of "micro-cladding"; or $A_c = A_m$. For this, H13 powder was used as a coating under 4340 steels. Laser cladding was performed with IPG top-hat laser with a maximum P of 1500 W and beam diameter (b_d) of 6 mm, coupled to Yaskawa arm. Producing line and area cladding tracks. Then, samples were characterized by optical microscopy, determining dilution (D), "HAZ angle" (α') and clad angle (α). As result, were determined parameters of E = 86.6%, v_s = 15 mm/s and μ = 6 g/min to produce a satisfactory micro-cladding with D ≈ 31% and α of 112.70°.*

Keywords: *micro-cladding, top-hat laser beam, robotic arm, laser beam, low power cladding processing*

1. INTRODUCTION

Surface improvements and additive manufacturing by laser cladding has a wide spectrum of applicability in heavy, marine, aeronautics and among others industries; considering a satisfactory anchorage between substrate-coating or additive layers coats due to metallurgical bonding occurrence (Vilar, 1999). According to Decker (1995), energy beam transference, must be enough to alter the physical state of cladding process materials. Acting with distributivity way between the coating powder and substrate materials; promoting a satisfactory diffusion and metallurgical bonding.

Li et al. (2019) highlights that extreme high speed laser application (EHLA), ensures a 60-80% energy for clad powder; enough for its melting before on substrate deposition. With this, a composite bonding assurance is more likely to laser-based directed energy deposition (DED-LB); or 20% of energy to the powder and 80% substrate (Sommer et al., 2021), which also imposes a greater heating, or modification of substrate microstructure. Likewise, powder feeder focus must be adjusted with beam focus of the laser beam; as well as the target focal for its best efficiency (Li et al., 2021). However, according to Li et al. (2019), even well adjusted, EHLA may be bringing negative repercussions, also modifying substrate microstructure due to high temperatures variations. In this sense, low-power laser methods or micro-cladding has been shown as an alternative for high temperature spread to the substrate (Lusquiños et al., 2009).

The literature shown the first researches on micro-cladding more than ten years ago, with investigations aiming on substrate thermal reducing propagation, applied to electronic paste and additive manufacturing (LμCDM) for micro-slots (Cai et al., 2009; Lusquiños et al., 2009; Yao et al., 2015). Where, a low power laser (50-200W) with small spots "b_d" (15-20um) are employed; usually coupled to computational numerical control (CNC) working table systems. Being

observed claddings with metallurgical bond and desired structural improvements, according to the research objective. Due to Gaussian beams transferring high energy density at small region near the center; without substrate thermal changes.

In fact, as stated by Keist and Palmer (2016), Gaussian profile lasers transfer a double of the power in 30% of their profile region, corresponding the nearing center. With this, for avoid larger heat propagation than substrate laser track, a low power and beam spot are conditioning parameters. Becoming a challenge for micro-cladding, even for pre-deposited powders (Cai et al., 2009). According to Yao et al., 2015, due to reduced sample area dimensions, the layout set-up becomes difficult, as well as to synchronize the powder feeder in EHLA and DED-LB systems, impacting the accuracy of the experiment. Thus, alternatives such as the use of top-hat or flat-top laser profiles becomes a feasible alternative, due to small Gaussian regions occurrence on the laser profile center (Tenbrock et al., 2020).

Hamburg (2012) states out that; in theory; the top-hat lasers deliver a uniform energy along the entire trapezoidal cross-section, guarantying a circular beam diameter impingement. Nevertheless, as noted by Tenbrock et al. (2020), in many cases occur a central energy diffuse region, similar to Gaussian profiles; containing peaks with smaller width than the beam and hardly noticeable length. However, as Tenbrock et al. (2020) stresses, these variations are imbued with high energy density; producing small cavities (A_p) below the substrate melting area (A_m). With this, top-hat parameters as efficiency (E); associated to laser power (P); as well scan speed (v_s) and powder feeding rate (μ) could be adjusted in order to use A_p as a melt zone with an equivalent cladding area (A_c); meeting Goodarzi et al. (2015) parameters of dilution (D) equation. In addition, the determination of clad angle (α); or heat affected zone angle (α'); according to Pellizzari et al. (2022) process; adjust the clad quality, determining best conditions for proper substrate/coating diffusion.

In this context, this present paper aimed to determine the parameters for micro-cladding with a top-hat laser. Using a SAE 4340 substrates and H13 powder for cladding. Where, the initial irradiation determined preliminary cladding parameters. Then, the cladding was carried out, determining new parameters. Thus, the samples were analyzed by optical microscope (OM) and microhardness Vickers profiling (MHV).

2. EXPERIMENTAL

Initially, the arm flange spatial arrangement, of the machine arm; as defined by programming frame tool used in the software; was obtained by universal serial bus (USB) transference. With this, were developed a computational interface by linear tracks programming, with only-irradiation starting parameters. From this starting analysis, the micro-cladding parameters were determined, including deposition rates parameters.

Sequentially, starting and micro-cladded samples were sectional sliced, Bakelite embedded and metallographically prepared with sandpapers grits of: 80, 120, 220, 320, 400, 600, 800, 1200; and 1 μm and 0.5 μm alumina polishing. And then, analyzed, determining the micro-cladding optimal parameters, considering a process chart imbued with OM aspects of dilution and clad angle.

2.1 Materials, equipment and software

For this evaluation, an SAE 4340 was used as a substrate, as 5,1±0,1 mm thick discoidal pre-polished specimen, from a metal dowel (25 mm of diameter); hot rolled and annealed (830-11° C with 20°/ h of rate); obtained from IEAv technical support department (SUTEC). In addition, a commercial H13 powder (PAC1476), supplied by PAC Co. was used as a cladding. Both materials meet the ASTM A29M (2004) and ASTM A681 (2008) composition parameters; and F3187 (2016) granulometry DED-LB criteria, for H13, as Figure 1 (A) and Table 1 shown. Likewise, the materials presented a predominance of quenched martensite (Fe-α'); typically founded in SAE steels, as Silva and Paredes (2016) stated; and elongated and angular grains, typically founded on metallic powders (Segura et al., 2019), as the SEM micrographs (SAE-1000X magnification and H13-125X) of Figure 1 (B and C, respectively) shown.

In addition, a Sigma 400Pro laboratory saw, an Aropol 2V polishing machine and Buehler mounting equipment were used for dowel slicing, Bakelite embedding, grinding and polishing preparation. Likewise, consumables are used as cloths and water sandpapers (Arotec), XAD16N Bakelite, alumina powders (Pace co.) and Marble reagent (Sigma Aldrich) for metallography. For irradiation and micro-cladding, a YLR-1500-MM-WC IPG Ytterbium fiber top-hat laser was used, with a spot "b_d" of 6 mm, wavelength "λ" of 1.07 μm and a maximum power "P" of 1500 W; as a flange tooling of a YRC1000 Yaskawa GP25 robotic arm, with EHLA feeding by a AT-1210 Thermach Inc. powder feeder, as the Figure 2 shown.

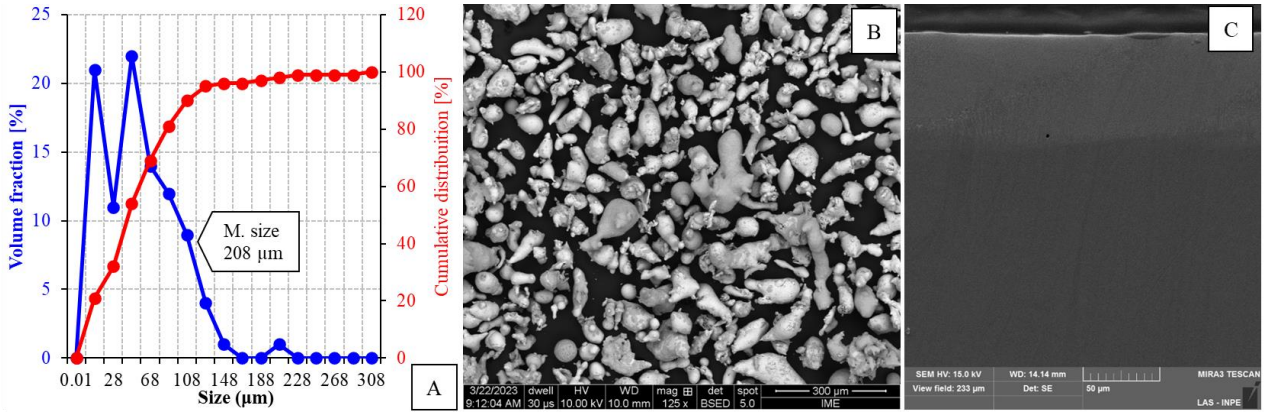

Figure 1. Materials granulometry and microstructure.

Table 1. Materials chemical composition.

Elements	**4340 Steel**		**H13**	
	Substrate	ASTM A29M Criteria	Cladding	ASTM A681 Criteria
	%W	W%	W%	W%
C	0.36	0.15-0.20	NI	0.32-0.45
Cr	0.79	NC[(2)]	4.89	4.75-5.50
Fe	95.80	NC	92.18	NC
Mn	0.64	0.70-1.00	NI	0.20-0.60
Mo	0.22	NC	1.41	1.10-1.75
Ni	1.70	NC	NI	NC
P	NI[(1)]	<0.04	NI	<0.03
S	NI	<0.05	NI	<0.03
Si	NI	NC	0.61	0.80-1.25
V	NI	NC	0.91	0.80-1.20

[(1)] unidentified; [(2)] no criteria

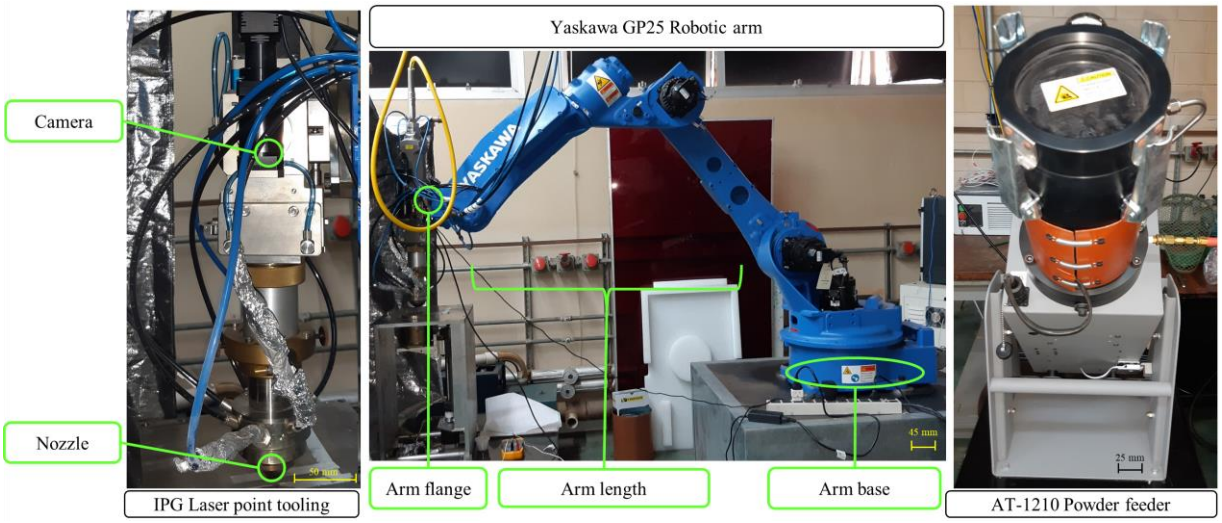

Figure 2. Robotic arm and powder feeder Illustrative pictures.

The laser cladding system were supported by peripheral such as an IPG Chiller system, Z-axis variation sample table, homemade powder exhauster and STC-HD203DV optical camera linked to a 32" Samsung monitor; as well as, argon gas for sample shielding and powder charging; with flow of "s_g" and "s_t", respectively. Noting that, personal protection equipment (PPE) were used for operation security as 10.6 µm wavelength factor sunglasses. In addition, the analyses were performed using a Zeiss microscope for OM and a FM-700 micro durometer for MHV test. For computational supporting, micrographs rasterizing and interface, a licensed TopSolid 7.16 and AutoCad 2020 software. Being calculated the measurements regarding the cladding or irradiation morphology and producing a “digital-mirror” substrates in

standard tessellation language "STL" archive format. In addition, RoboDk software was used for the laser tracks creation under the STL substrate; with implementation of output program for machine.

2.2 Methods

Irradiations and preliminary claddings were performed with H13 on SAE 4340 substrates, with initial parameters of "v_s" scan speed, "E" power efficiency and "μ" powder deposition rate. From this preliminary cross section samples analysis; by OM; were noted small "A_p" regions below "A_m" clad diffusion region. According to Homburg and Mitra (2012), the centered Gaussian on top-hat laser beam, enables the micro-cladding parameters development, as shown Figure 3; which also contemplates these first parameters and others obtained variables as: "A_{HAZ}" heat affected zone HAZ area.

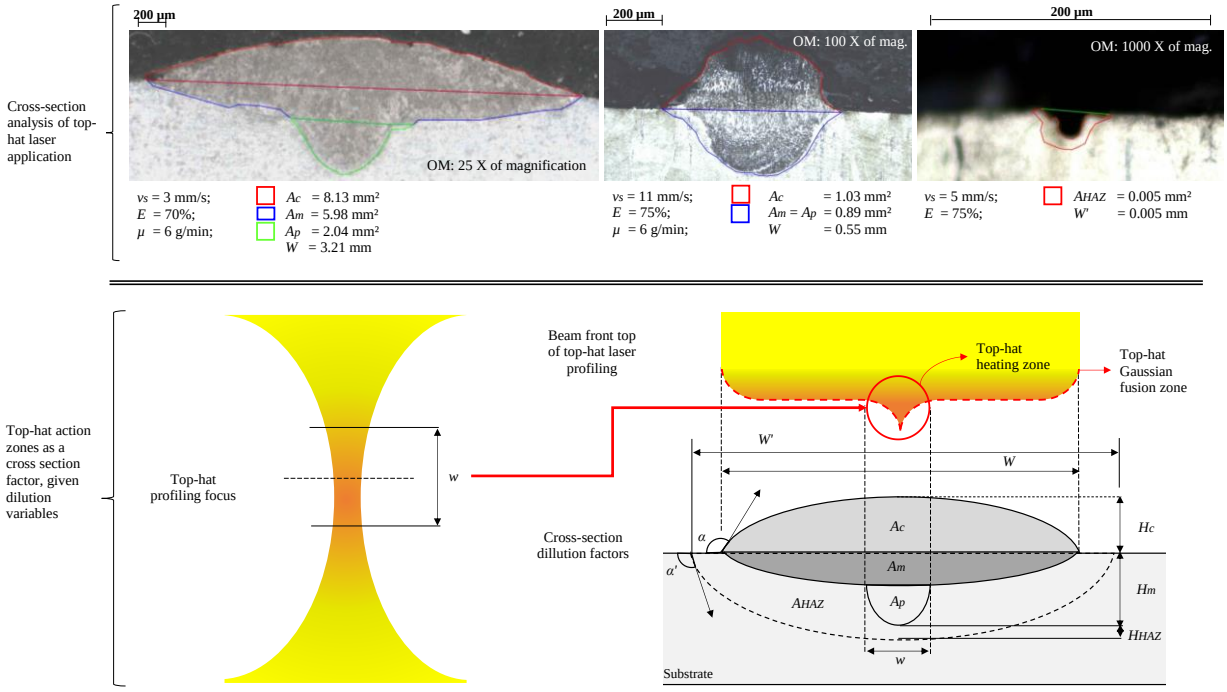

Figure 3. First observations of the top-hat laser Gaussian effect with graphical explanation schemes.

As the Figure 2 graphical scheme shown; according to empirical observations and Homburg and Mitra's (2012) concepts; the top-hat Gaussian region prints a higher temperature region with "w" diameter, equivalent to width of A_p. In this case, variables such as HAZ depth "H_{HAZ}" and width "W"' are related to a given HAZ angle "α"'. Just as the dilution variables, such as cladding height "H_c" and diffusion depth "H_m" relate to Dilution (D) and clad angle (α), from Goodarzi's et al. (2015) Eq (1) and (2). According to Pellizzari's et al. research (2022), D and α (or α') define the best cladding conditions, being analyzed with a "process-chart" containing OM cross-section micrographs. In this way, SAE's irradiation starting parameters were defined; considering high v_s speeds and E variation range of 30-86%. With this, only a HAZ region were ensured without a fusion or melted pits regions, as the Table 2 shown. Noting that in this table, the nomenclatures of the first tracks and substrates used are defined. In addition, was done irradiation (μ = 0), with one laser pass under each track.

$$\boldsymbol{D} = A_m(A_C + A_m)^{-1}\,, \tag{1}$$

$$\propto = 180 - 2\tan^{-1}([2H_c][W]^{-1}); or\ \propto' = 180 - 2\tan^{-1}([2H_{HAZ}][W']^{-1})\,, \tag{2}$$

From these initial irradiations (4 tracks per substrate) were obtained and applied H_{HAZ} and W' variables on Eq. (2); in order to compare to Pellizzari's et al. (2022) parameters for the best α' results. Furthermore, these results were related to radiance (I_0), energy density; or fluency; (E_D) and optimal scan speed (ov_s), according to equations (3) and (4) of Decker (1995), Keist, Palmer (2016), Santos (2017) and Tenbrock et al. (2020).

Table 2. Irradiation starting parameters.

Nomenclatures		**Laser passages**	**Variable Parameters**			**Fixed parameters**	
Tracks	Substrate		v_s	E	μ	P	b_d
			mm/s	%	g/min	W	mm
TR1	1	1	25.00	36.10	0	1500.00	6.00
TR2		1		45.80	0		
TR3		1		68.80	0		
TR4		1		86.60	0		
TR5	2	1	18.00	86.60	0		
TR6		1		68.80	0		
TR7		1		45.80	0		
TR8		1		36.10	0		

Therefore, micro-cladding new parameters were defined, contemplating deposition and irradiation tracks, besides a 20X20 mm superficial coating, as Table 3 shown. Noting that the variables of Eq. (3) to (5) referred to spot diameter, considering experiment initial "T_i" and final "T_f" temperatures; besides the SAE 4340 properties of density "ρ" and specific heat "C_p". In addition, Table 3 also contemplates these final tracks and substrates nomenclatures; with number of passages of laser; only an irradiation pass (μ = 0) or both irradiation and deposition passages, per track or surface.

$$I_0 = [2EP][\pi(0.5b_d)^2]^{-1} \tag{3}$$

$$E_D = [4EP][\pi b_d v_s]^{-1} \tag{4}$$

$$ov_s = [EP]\left[\pi(b_d)^2 \rho C_p\left(T_f - T_i\right)\right]^{-1} \tag{5}$$

Table 3. Irradiation and micro-cladding final parameters.

Nomenclatures		**Laser passages**	**Variable Parameters**			**Fixed parameters**	
Tracks	Substrate		v_s	E	μ	P	b_d
			mm/s	%	g/min	W	mm
TR9	3	1	9.00	86.60	0	1500.00	6.00
		1	9.00	86.60	6.00		
TR10	4	1	11.00	86.60	0		
		1	11.00	86.60	6.00		
TR11	5	1	15.00	86.60	0		
		1	15.00	86.60	6.00		
TR12	6	2	11.00	86.60	0		
SUR1	7	1	11.00	65.00	0		
		1	11.00	65.00	5.20		

Therefore, for each micro-cladding process, the initial irradiation passage acted as a substrate preheating, ensuring the cladding anchorage; or promoting fusion on irradiance only, as illustrated by Figure 4 photographs.

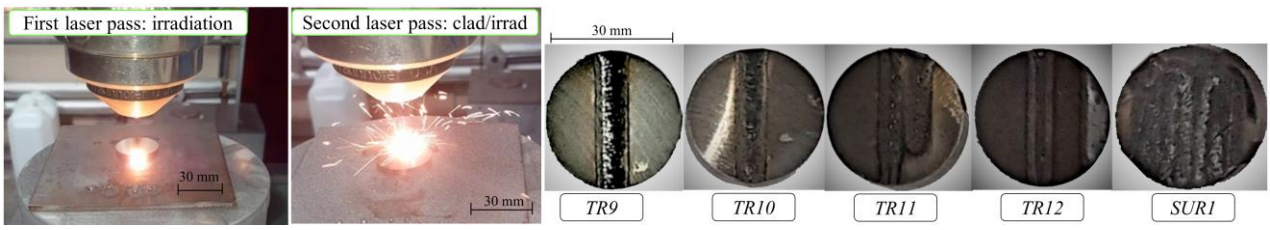

Figure 4. Laser passes development and coated samples.

In parallel, 5X25 mm discoidal STLs were built in TopSolid. Then, two programs were implemented in RoboDk: single line "P_1" and 20mm length segments, off-set by 3mm "P_2"; or a 50% of tracks overlapping. Considering that P_1 and P_2 were based on real Yaskawa arm coordinates; or "home position", as shown in the codes below:

Intro	Positions	Commands
/JOB	C00000=1167,25485,-36793,680,37444,-430	MOVJ C00000 VJ=1.00
//NAME P1	C00001=1187,29133,-45059,569,44443,-358	MOVJ C00001 VJ=1.00
//POS	C00002=1535,47258,-50639,-1402,55783,405	MOVJ C00002 VJ=1.00
///NPOS 4,0,0,0,0,0	C00003=4395,47430,-50420,-4016,55790,1162	TIMER T=3.00
///TOOL 0		MOVL C00003 V=9.0
///POSTYPE PULSE		
///PULSE		
//INST		
END		
/JOB	C00000=1589,39507,-46190,-1588,49025,539	MOVJ C00000 VJ=1.00
//NAME P2	C00001=1618,38618,-49596,-1579,50674,517	MOVJ C00001 VJ=1.00
//POS	C00002=1535,47258,-50639,-1402,55783,405	MOVJ C00002 VJ=1.00
///NPOS 14,0,0,0,0,0	C00003=2966,47324,-50556,-2710,55786,784	TIMER T=3.00
///TOOL 0	C00004=2958,47658,-50129,-2705,55694,784	MOVL C00003 V=11.0
///POSTYPE PULSE	C00005=1530,47592,-50213,-1400,55692,406	MOVL C00004 V=11.0
///PULSE	C00006=1526,47926,-49786,-1398,55600,406	MOVL C00005 V=11.0
//INST	C00007=2949,47991,-49703,-2701,55603,785	MOVL C00006 V=11.0
END	C00008=2941,48325,-49275,-2696,55511,785	MOVL C00007 V=11.0
	C00009=1522,48261,-49358,-1395,55508,406	MOVL C00008 V=11.0
	C00010=1518,48595,-48929,-1393,55416,407	MOVL C00009 V=11.0
	C00011=2933,48659,-48847,-2692,55418,786	MOVL C00010 V=11.0
	C00012=2925,48993,-48417,-2687,55325,787	MOVL C00011 V=11.0
	C00013=1514,48929,-48500,-1391,55323,407	MOVL C00012 V=11.0
		MOVL C00013 V=11.0

Where: home position; joint movement; joint velocity; laser actuation timer; linear movement; linear speed = v_s

Figure 5, in turn, illustrates the RoboDK computing environment, such as STL, P_1 and P_2 program path, virtual work station, and Yaskawa arm and IPG laser virtual versions.

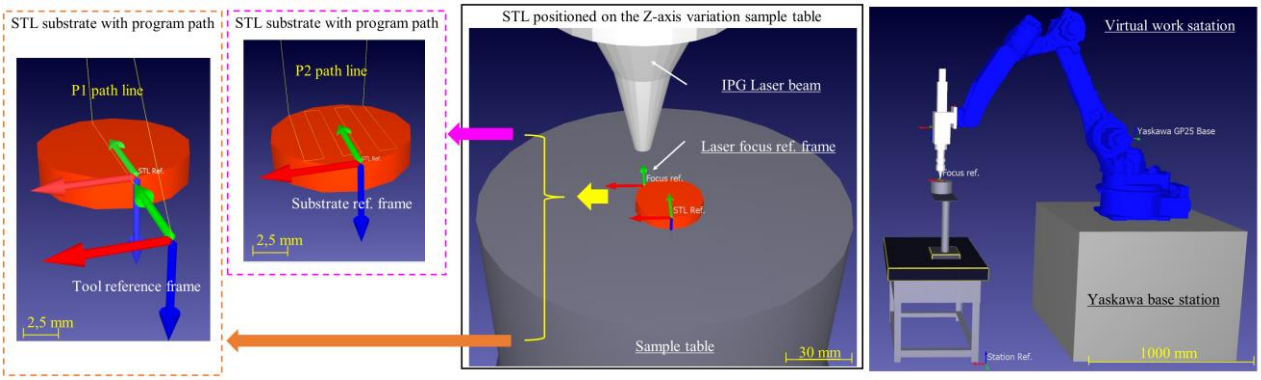

Figure 5. Images of Work station and STL substrate RoboDk generated.

3. COMMENTED RESULTS

From initial irradiation analysis (Table 2), it commented this parameters assertiveness choosing. Since, α'; according to Table 4; remained within the criteria of Pellizzari et al. (2022) for *TR-3, 4* and *6*; being obtained from the analysis of the process chart of Figure 6. For this purpose, it is commented that "ov_s" determined a maximum between 18-22 mm/s. Where the MHV test; according to Figure 7; confirms the best performance of these tracks. However, considering the required EHLA power distribution of 80/20%; it was coherent the vicinal "v_s" of 9-11 mm/s choosing.

In fact, these parameters were confirmed, as Table 5 and the process chart in Figure 8 shown. Where the *TR-9* and *10* tracks obtained well α results (Pellizzari et al., 2022); with "*TR9*" getting the best results, being used on "*SUR1*" surface. With the $\mu = 6$ *g/min*, previous observed, also showing assertive parameters for micro-cladding. For "*D*", nevertheless, weren't observed "well" results, according to literature (Goodarzi et al., 2015; Pellizzari et al., 2022). This occurrence could be explained by the coating and substrate chemical similarity (steel under steel), allowing a high diffusibility between them. With this, the α analysis is the main boundary condition for best parameters determination; considering this experiment conditions. In the Figure 8 process chart horizon, on the other hand, were observe that the

despite *TR-12* being outseeing from *D* and α criteria (Pellizzari et al., 2022), it was the only track that obtained the real micro-cladding conditions: A_p equivalent to A_m. With the Figure 9 MHV test result evidencing this performance.

Table 4. Irradiation morphology results for first parameters.

Tracks	***W'*** mm	H_{HAZ} mm	A_{HAZ} mm²	***α'*** grade	I_0 W/cm²	E_D W.s/cm²	ov_s mm/s	T_i °C	T_f °C	C_P J/kg.K	***ρ*** Kg/m³
Criteria [1]:				149-162							
TR1	0.01	0.006	0.0008	167.56	1915.16	229.82	9.47				
TR2	0.02	0.006	0.0010	167.29	2429.77	291.57	12.01				
TR3	0.03	0.013	0.0033	155.88	3649.95	437.99	18.05				
TR4	0.05	0.018	0.0069	149.16	4594.27	551.31	22.72	27	1427	460	7.85
TR5	0.26	0.025	0.0482	139.30	4594.27	765.71	22.72				
TR6	0.04	0.016	0.0053	152.69	3649.95	608.33	18.05				
TR7	0.02	0.008	0.0015	164.14	2429.77	404.96	12.02				
TR8	0.02	0.006	0.0010	168.65	1915.16	319.19	9.47				
[1]	Pellizzari et al. (2022)										

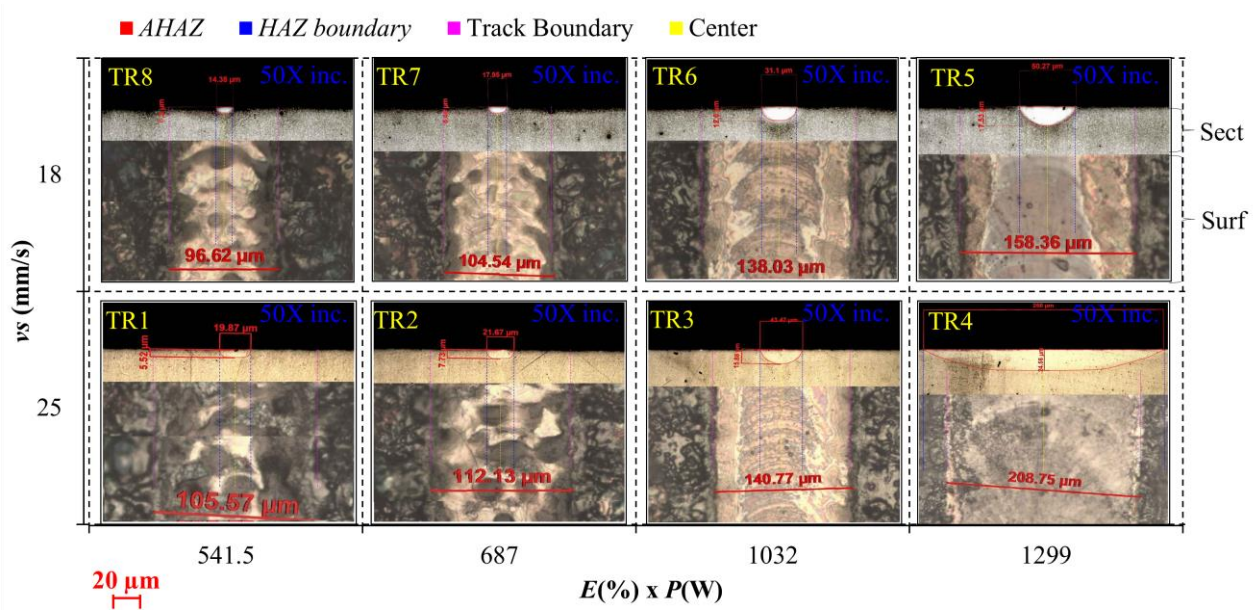

Figure 6. Flowchart process of initial irradiation parameters.

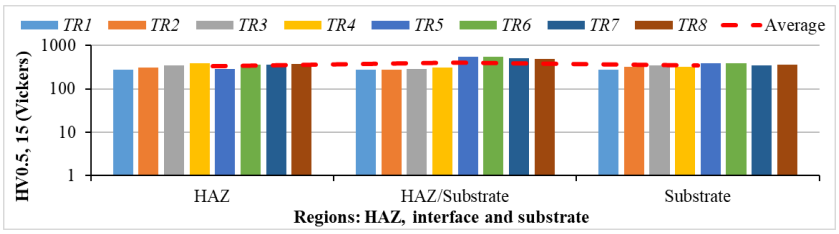

Figure 7. MHV test graph for *TR1* to *TR8* samples.

As commented, in Table 5 its observed "I_0" and "E_D" as laser fixed parameter function; without A_{HAZ} and "*w*" influence; with no considerate the micro-cladding process. Since, the Eq. (3) and (4) only includes the laser beam fixed parameters as: b_d, *E* and *P*. In this way, an exclusive top-hat laser equation are suggested for further studies. In the Figure 6 flowchart process, on the other hand, the high A_{HAZ} for *E* of 86.6% stands out; indicating that it's a power threshold.

In this sense, the pair $\{v_s, E\} = \{15, 86.6\}$ produced a micro-cladding in *TR12*; with the highest microhardness. Although, this pair wasn't used in *SUR1*. However, *SUR1* had a thin thickness surface; of the order of 300 µm; as a micro-cladding propertie. Furthermore, this surface presented a well uniformity; as observed in Figure 10 MO micrograph. In addition, presented a satisfactory microhardness, as Figure 11 graph shown.

Table 5. Irradiation and micro-cladding morphology results for final parameters.

Tracks	***W*** mm	***Hc*** mm	***Ac*** mm²	***Hm*** mm	***Am*** mm²	***Hp*** mm	***Ap*** mm²	***w*** mm	***D*** %	***α*** grades
Criteria [1]:									8-14	149-162
TR9	3.22	0.32	0.63	0.17	0.42	0.21	0.09	0.52	44.23	157.22
TR10	2.40	0.16	0.32	0.15	0.27	0.20	0.06	0.47	51.13	150.37
TR11	0.36	0.12	0.03	0.06	0.01	0.07	0.01	0.36	31.50	112.06
SUR1	20,00	0.38	3.49	0.33	2.37				40.47	175.63
SUR (one-track)	3.33		0.58	0.05	0.39					

Tracks	***W'*** mm	***AHAZ***	***HHAZ***	***α'*** grade
Criteria [1]:				149-162
TR12	2.1	1.05	0.67	115.09

[1] Pellizzari et al. (2022)

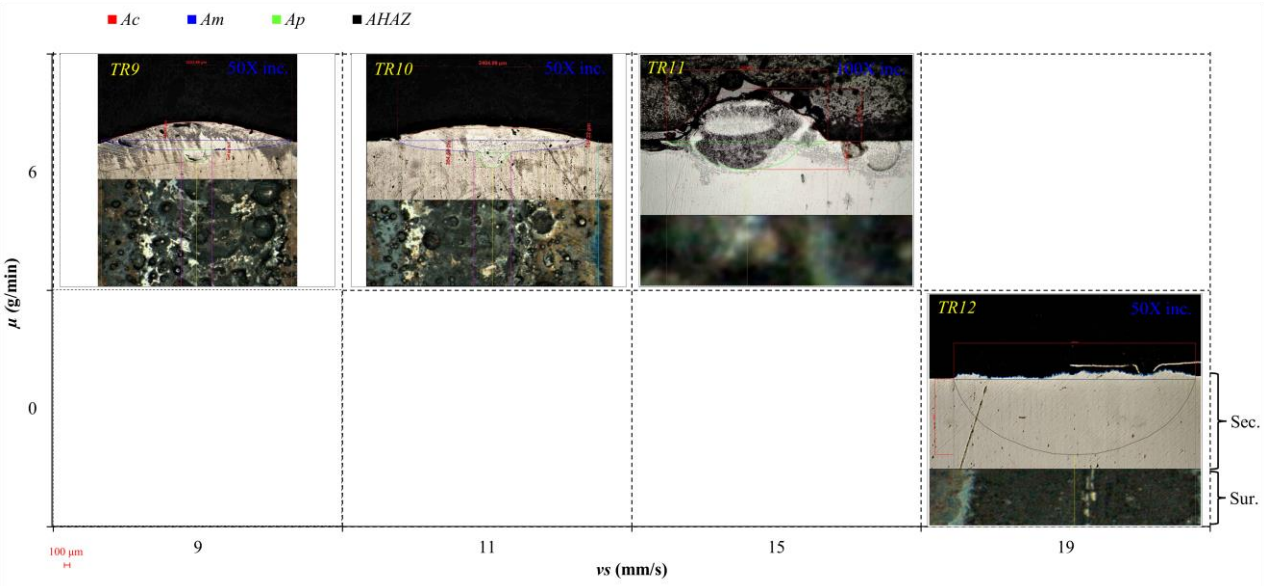

Figure 8. Flowchart process of final irradiation and cladding parameters.

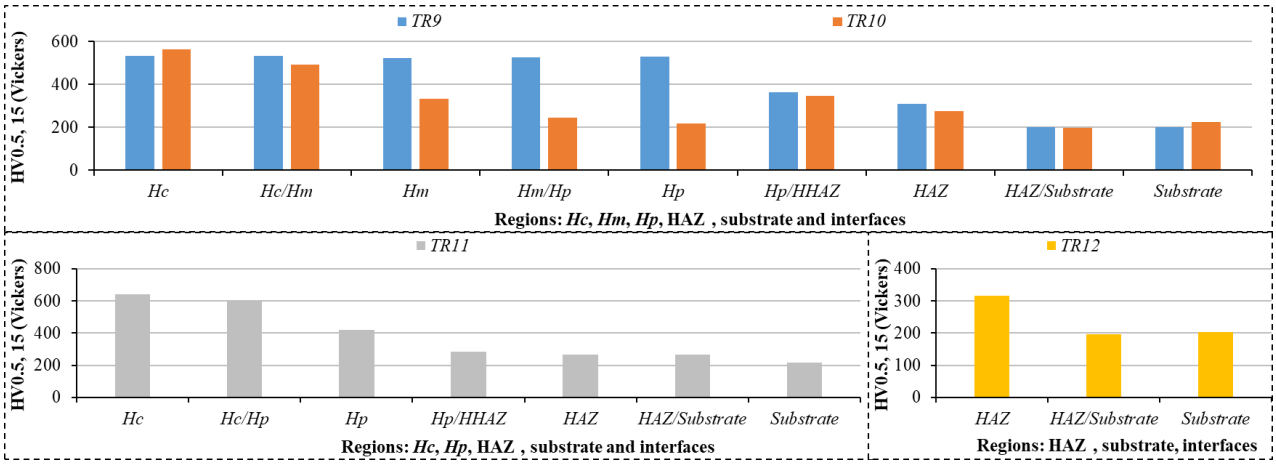

Figure 9. MHV test graph for *TR9* to *TR12* samples.

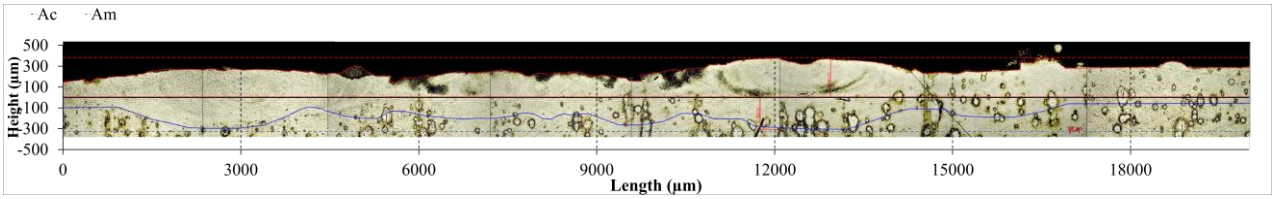

Figure 10. OM micrograph of *SUR1* profile.

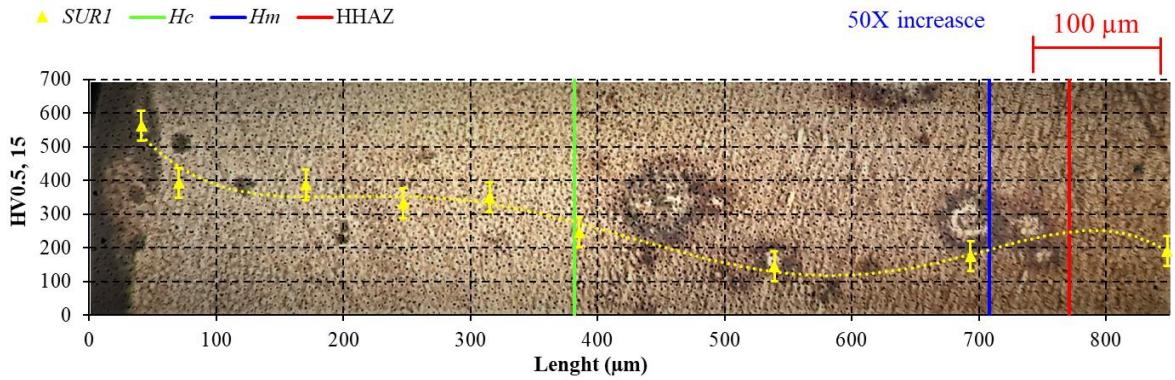

Figure 11. MHV test profile graph of *SUR1* sample.

4. FINAL CONSIDERATIONS

From these results, it can be concluded that it was possible to determine micro-cladding parameters. These coatings presented superior hardness, indicating a well cladding quality. Similarly, it was possible to coating a surface with parameters close to *TR12*, indicating this efficient for coat production. "*SUR1*" still obtained a thin average thickness; of about 300 µm. Without of many cracks and macro-pores occurrence; with a satisfactory hardness. Indicating the success of the micro-cladding acting as a coat layer. However, still necessary the investigation of *TR12* parameters acting as a surface. Furthermore, other chemical and mechanical analyses are required for further studies; in order to continue this researching.

5. ACKNOWLEDGEMENTS

We thank to Instituto de Estudos Avançados Instituto Militar de Engenharia, Instituto Tecnológico de Aeronáutica, and Instituto Nacional de Estudos Espaciais for support team and facilities. This work was funded by CNPq, under the grant: 405624/2022-0; CAPES, under the grant: 88887.285953/2018-00, and FINEP, under the grant: 25670-SUB-1.

6. REFERENCES

American Society for Testing and Materials , 2008, ASTM A68: standard specification for tool steels alloy, West Conshohocken, PA, 19428-2959 USA.

American Society for Testing and Materials, 2004, ASTM A29M: standard specification for steel bars, carbon and alloy, hot-wrought, general requirements for steel bars, carbon and alloy, hot-wrought, West Conshohocken, PA, 19428-2959 USA.

American Society for Testing and Materials, 2016, F3187: standard guide for directed energy deposition of metals, West Conshohocken, PA, 19428-2959 USA.

Cai, Z., Li, X., Hu, O., Zeng, X., 2009, Fabrication of microheater by laser micro cladding electronic paste, Materials Science and Engineering B, Vol. 157, pp. 19.

Decker, F. .J., 1995. "Beam distributions beyond RMS". In *Proceedings of the AIP Conference Proceedings 1995*.

Goodarzi, D. M., Pekkarinen, J., Salminenet, A., 2015, Effect of process parameters in laser cladding on substrate melted areas and the substrate melted shape, Journal of Laser Applications, Vol. 27, pp. 1387.

Homburg, O., Mitra, T., 2012, "Gaussian-to-Top-Hat Beam Shaping – An Overview of Parameters, Methods and Applications", In *Proceedings of the LIMO Lissotschenko Mikrooptik GmbH, Bookenburgweg 4-8, 44319*, Dortmund, Germany.

Keist, J. S., Palmer, T. A., 2016, Role of geometry on properties of additively manufactured Ti-6Al-4 V structures fabricated using laser based directed energy deposition, Materials Design.

Li, L., Shen, F., Zhou, Y., Tao, W., 2019, Comparative study of stainless steel AISI 431 coatings prepared by extreme-high-speed and conventional laser cladding, Journal of Laser Applications, Vol. 31.

Li, T., Zhang, L., Bultel, G. G. P., Schopphoven, T., Gasser, A., Schleifenbaum, J. A., Poprawe, R., 202, Extreme High-Speed Laser Material Deposition (EHLA) of AISI 4340 Steel, Coatings, Vol. 9, pp. 778.

Lusquiños, F., Comesaña, R., Riveiro, A., Quintero, F., Pou, J., 2009, Fibre laser micro-cladding of Co-based alloys on stainless steel, Surface & Coatings Technology, Vol. 203, pp. 1940.

Pellizzari, M., Zhao, Z., Bosetti, P., Periniet, M., 2022, Optimizing direct laser metal deposition of H13 cladding on CuBe alloy substrate, Surface & Coatings Technology, Vol. 432, pp. 128084.

Santos, C.L., 2017. *Study of the Deposition Process of Stellite 6 with a 125W CO_2 Laser*. Ph.D. thesis, Graduate Program in Applied Physics and Mathematics, Aeronautical Technological Institute, São José dos Campos, Brazil.

Segura, I. A., Murr, L. E., Terrazas, C. A., Bermudez, D., Mireles, J., Injeti, V. S. V., Li, K., Yu, B., Misra, R. D. K., Wicker, R. B., 2018, Grain boundary and microstructure engineering of Inconel 690 cladding on stainless-steel 316L using electron powder bed fusion additive manufacturing, Journal of Materials Science and amp; Technology.

Silva, V. C., Paredes, R. S. C., 2016, Avaliação da relação Creq. / Nieq. para o revestimento AF2209 depositado por aspersão térmica com e sem pré-aquecimento, Revista Matéria, Vol. 21, pp. 481.

Sommer, N., Stredak, F., Böhm, S., 2021, High-Speed Laser Cladding on Thin-Sheet-Substrates—Influence of Process Parameters on Clad Geometry and Dilution, Coatings, Vol. 11, pp. 952.

Tenbrock, C., Fischer, F. G., Wissenbacha, K., Schleifenbaum, J. H., Wagenblast, P., Meiners, W., Wagnerb, J., 2020, Influence of keyhole and conduction mode melting for top-hat shaped beam profiles in laser powder bed fusion, Journal of Materials Processing Tech., Vol. 278, pp. 116514.

Vilar, R., 1999, Laser cladding, Journal of Laser Applications, Vol. 11, pp. 346.

Yao, B., Ma, X-L., Feng Lin, F., Ge, W-J., 2015, Microstructure and mechanical properties of Ti-6Al-4V components fabricated by laser micro cladding deposition, Rare Metals.